Research Article
Theme: Inhaled Drug Delivery of Biologics for Therapeutic and Vaccination

PEGylated Lecithin-Chitosan Nanoparticle–Encapsulated Alphα-Terpineol for *In Vitro* Anticancer Effects

Bahar Zarei,[1] Masoud Homayouni Tabrizi,[1,2] and Amir Rahmati[1]

Abstract. The aim of this study was to fabrication PEGylated lecithin-chitosan nanoparticles (PLC-NPs) as alphα-Terpineol's (αT-PLC-NPs) delivery system and examine its anti-cancer effects. αT-PLC-NPs were synthesized by self-assembling method; after characterization, entrapment efficiency of α-T was measured by HPLC procedure. MTT test was conducted for cytotoxicity evaluation. Chick chorioallantoic membrane (CAM) and quantitative polymerase chain reaction (qPCR) analysis were used to determine the angiogenesis properties, and qPCR, flow cytometry, and acridine orange and propidium iodide (AO/PI) staining were used to evaluate the pro-apoptotic effects of αT-PLC-NPs. Finally, the anti-inflammatory and antibacterial activity of the αT-PLC-NPs was also evaluated. αT-PLC-NPs with a size of 220.8 nm, polydispersity index (PDI) of 0.3, zeta potential of +29.03 mV, and encapsulation efficiency of 82% showed higher inhibitory effect on MCF7 cells (IC$_{50}$: 750 μg/mL) compared to HFF cells (above 1000 μg/mL). Decreased angiogenesis indices and embryonic growth factors in CAM assay, decreased expression of VEGF and VEGF-R genes, and decreased cell migration showed the inhibitory effect of αT-PLC-NPs on angiogenesis. Increased expression of P53, P21, and caspase9 genes, as well as the results of AO/PI staining along with increasing the number of SubG1 phase cells in flow cytometry, confirmed the pro-apoptotic effects of αT-PLC-NPs. Also, its anti-inflammatory effects were demonstrated by inhibiting the expression of pro-inflammatory cytokines (TNF-α and IL-6). The inhibitory power of αT-PLC-NPs in suppressing gram-positive and negative bacterial strains was demonstrated by disk diffusion (DD), minimum inhibitory concentration (MIC), and minimum bactericidal concentration (MBC) methods. PLC-NPs are a promising carrier for α-T transfer for preclinical studies.

KEY WORDS: alphα-Terpineol; PEGylated lecithin-chitosan nanoparticles; apoptosis; cytotoxicity; angiogenesis; antibacterial.

INTRODUCTION

Cancer is a multifactorial disease caused by abnormal and uncontrolled cells growth that usually leads to tumor formation (1). Breast cancer is classified based on the expression of molecular markers including estrogen, progesterone, and human epidermal growth factor receptors. Hormone receptor-positive breast cancer is the most common cancer and triple-negative is the most aggressive type of cancer (2). Oxidative stress and its damage play a critical role in the onset of malignancy of cells (3), so one of the most important strategies to prevent cancer is to use antioxidant compounds to remove extra free radicals and prevent damage to bio-macromolecules (4). Conversely, in the cancer treatment approach, one of the most important strategies used to inhibit cancer cells is to increase the amount of ROS and increase oxidative stress, followed by launching of the cell death signal pathway (5). Induction of oxidative stress (6), induction of apoptosis (7), and inhibition of angiogenesis (8) are important and practical strategies in the treatment of cancer cells with conventional methods such as chemotherapy.

However, side effects (9), lack of targeted treatment (10), and drug resistance (11) are some of the limitations of this treatment. The use of natural compounds and their effective transfer to target locations can play an effective role in removing such limitations. Alpha terpineol (monoterpenoid alcohol) is a major component of plant essential oils and has anti-cancer (12), anti-inflammatory (13), antioxidant (14), anti-bacterial (15), and anti-fungal effects (16). Increasing the delivery efficiency of bioactive compounds to cancer cells using nanocarriers can prevent them from interacting with

[1] Department of Biology, Mashhad Branch, Islamic Azad University, Mashhad, Iran.
[2] To whom correspondence should be addressed. (e–mail: mhomayouni6@gmail.com; mhomayouni6@mshdiau.ac.ir)

normal cells and limit possible side effects. Also, increasing the bioavailability, solubility, and effectiveness of treatment is another benefit of using nanocarriers in the transport of bioactive compounds [17].

Lecithin/chitosan nanoparticles are a colloidal carrier system and a suitable alternative to polymer NPs, solid lipid NPs, liposomes, and nanoemulsions. The negative and positive charges of lecithin and chitosan (respectively) cause the supramolecular self-regulation of these nanoparticles [18]. Lecithin is a safe and biocompatible substance composed of a mixture of phospholipids, mainly phosphatidylethanolamine and choline, and is commonly used in the preparation of other nanosystems [19, 20]. Chitosan is a natural polymer with a positive charge, limited immunogenicity [21], and high bioavailability and biocompatibility [22] that is able to bind to the negatively charged cancer cells and release the drug to the acidic pH tumor microenvironment. The pH response method of chitosan makes it appropriate as a drug delivery system for the cancer therapy [23]. Encapsulation of lipophilic compound in the hydrophobic lipid core by physical method or high-efficiency electrostatic interactions [24] and coating of these nanoparticles with chitosan polymers with increased adhesion and mucosal penetration properties can increase the shelf life and strengthen the penetration of the drug [25, 26]. Polyethylene glycol (PEG) as a synthetic polymer for chemical modification of nanocarrier surfaces can play an effective role in reducing immunogenicity, increasing the half-life of carriers in the bloodstream, and increasing the accumulation of NPs at the site of tumors under the influence of EPR [27]. Modifying the surface of nanoparticles with PEG (PEGylation) prevents the interaction of blood components and plasma proteins with the surface of NPs in biological environments and thus reduces the interaction of nanocarriers with opsonins and the removal of NPs by the reticuloendothelial system [28].

Due to the possibility of loading α-T as a lipophilic compound in the lipid section of hybrid nanoparticles and the possibility of chemical modification of nanoparticles with synthetic polymers to increase its transfer efficiency, in this study, for the first time, α-T was loaded on LC-NPs. Then, the surface of the NPs was modified with PEG. Finally, the effect of αT-PLC-NPs on inhibiting MCF-7 cancer cells was evaluated based on angiogenesis and apoptosis mechanisms.

MATERIALS AND METHODS

Materials

Alphα-Terpineol (α-T), poly lactic-co-glycolic acid (PLGA), polyvinyl alcohol (PVA), low molecular weight (LMW) chitosan, folic acid (FA), propodium iodide (PI), and acridine orange (AO) were purchased from Sigma-Aldrich. Dichloromethane (DCM), 3-(4,5-dimethylthiazol-2-yl)-2,5-diphenyl-2H-tetrazolium bromide (MTT), 2,2-diphenyl-1-picrylhydrazyl (DPPH), 2,2′-Azino-bis(3-ethylbenzothiazoline-6-sulfonic acid) (ABTS), potassium persulfate, and dimethyl sulfoxide (DMSO) were purchased from Merck Co. All the materials needed for cell culture were purchased from Invitrogen Co. Breast cancer (MCF-7) and skin fibroblasts (HFF) cell lines were purchased from Ferdowsi University of Mashhad cell bank, Iran.

Preparation of αT-PLC-NPs

First, CS (0.2% W/V) was added to 1% acetic acid and incubated on stirrer at 60 ° C (2 h). Then, lecithin with a ratio of 15 to 1 relative to chitosan was added to ethanol and, after dissolution, α-T was added to the lecithin/ethanol mixture. After moderate stirring for 5 min, the mixture of lecithin and α-T dropwise was added to the CS solution on the stirrer (30 min); then, the PEG dissolved in water dropwise was added to the above solution and probe sonicated (2 min); the final solution was centrifuged (30 min at 13,000 rpm). The supernatant was collected to evaluate the amount of encapsulated α-T and the resulting precipitate was lyophilized. To lyophilize the NP suspensions without cryoprotective agents, they were frozen at −196 °C for 3 h. After freezing, NP dispersions were transferred into a −50 °C at a pressure of 0.07 mbar for 24 h. The samples were then stored at −20 ° C for 8 h and stored at 4 °C until further use.

Physicochemical Characterization of αT-PLC-NPs

Z average, PDI, and ζ-potential of αT-PLC-NPs were examined by DLS methods. To its measure, 1 mg of αT-PLC-NPs was diluted with 100 mL of distilled water (DW) and analyzed in a 175° scattering angle in the temperature of $25 \pm 0.5°C$. FESEM was used to assess the morphology of αT-PLC-NPs. For this purpose, a few drops of the diluted αT-PLC-NPs in DW (1 mg/10 mL) were transferred on aluminum foil and then dried. The surface of the samples was then coated with gold and imaged under a FESEM microscope. FTIR was used to examine the functional groups and bonds in the structure of αT-PLC-NPs. For this purpose, 2 mg of αT-PLC-NPs was combined with potassium bromide (KBr) and, after compression and conversion into thin tablets, it was placed in the device and scanned.

Determination of α-T Loading

In this study, an indirect method was used to evaluate the encapsulation efficiency of α-T [29]. For this purpose, the supernatant collected from the last stage of synthesis was analyzed by HPLC method. Indirect analysis was performed by reverse phase chromatography which is based on the amount of αT in the supernatant. The amount of encapsulation was done by analyzing the sub-peak level of the test sample in comparison with the standard sample. EE % = (Entrapped α-T)/(Total α-T)×100%.

Evaluation of the Release of α-T

Twenty milligrams of αT-PLC-NPs was dissolved in 10 mL of PBS (PH: 7.4) and gently shaken. At specific times (0.5, 1, 12, 24, 48, 72, and 96 h), 1 mL of the solution was removed and replaced with an equal volume of fresh medium. The collected medium was centrifuged (9000 rpm for 5 min) and the supernatant was used to evaluate the release rate. The α-T released from nanoparticles was calculated using the following formula: the cumulative amount of α-T released at each sampling time point (Mt)/the initial weight of the α-T-loaded in the sample (M0)× 100 [30].

Antioxidant Assay

ABTS Scavenging Assay

For this purpose, first ABTS free radicals were obtained by mixing 2 mL of ABTS (7 mM) and 1 mL of potassium persulfate (2.45 mM) and incubation for 16 h in the dark at 25 °C. Then, the resulting solution was diluted with DW to reach absorption of 0.756 at a wavelength of 743 nm. To evaluate the scavenging power of αT-PLC-NPs, first 500 μL of different concentrations of αT-PLC-NPs was prepared by serial dilution and then 500 μL of ABTS free radicals was added to each microtube and, after incubation (1 h) in the dark, the absorption of samples was measured by a spectrophotometer at a wavelength of 734 nm (5). The rate of ABTS free radical inhibition was calculated using the following formula:

$\%\text{ABTS free radical scavenging} = OD_{control} - OD_{sample}/OD_{control} \times 100$

DPPH Assay

To evaluate the inhibitory power of $DPPH^{\cdot+}$ by αT-PLC-NPs, serial dilutions of αT-PLC-NPs with a volume of 500 μL were prepared, and then an equal volume of solution containing DPPH free radicals was added to each microtube. After 30-min incubation (37° C), the adsorption of the samples at 517 nm was evaluated and the percentage of DPPH free radical scavenging was determined using the following formula (5).

$\%\text{DPPH free radical scavenging} = OD_{control} - OD_{sample}/OD_{control} \times 100$

Cell Viability Assays

The toxicity of α-T, PLC-NPs, and αT-PLC-NPs against MCF-7 cancer cells was evaluated compared to HFF cells by MTT method. For this purpose, the 5×10^3 cells/well was seeded on 96-well plates and after 24 h was treated. Forty-eight hours later, the treatment medium was drained and 20 μL of MTT solution was added to each well. Incubation was performed for 4 h to complete the reaction, after which the MTT medium was removed and DMSO (100 μL) was added to wells. Finally, the absorbance of the samples was recorded at 570 nm and the cell viability percentage was calculated using the following formula (31).

$\%\text{Viability of cells} = OD_{sample}/OD_{control} \times 100$

In Vivo and In Vitro Assay for Angiogenesis

In order to examine the effects of αT-PLC-NPs on angiogenesis, the CAM method was used as an *in vivo* method. Next, the expression of angiogenesis-related genes in chorioallantoic membranes was evaluated by qPCR method. Scratch test was used to investigate the effect of αT-PLC-NPs on cell migration.

CAM Assay

Fifty Ross fertilized chicken eggs were obtained from Toos Poultry Farm in Mashhad and, after disinfection, were transferred to the incubator (37 °C, 85–90% humidity). Forty-eight hours later, an air chamber was created in the lateral shell of the eggs; then, the window was blocked with special glue and paraffin, and the eggs were transferred to the incubator. Samples were treated with different concentrations of αT-PLC-NPs on the eighth day. For this purpose, a window was opened in the eggshells, and after placing the gelatin sponge on the chorioallantoic membrane, 10 μL of different concentrations of αT-PLC-NPs was loaded on the gelatin sponges; then, the windows were closed again and the eggs were transferred to the incubator. Four days after treatment, the chamber was opened on the samples shell and was imaged using a stereomicroscope. The prepared images were analyzed (image J software) to evaluate the mean length and number of blood vessels. Scales and calipers were used to assess fetal growth factors, including fetal weight and height (9).

Gene Expression

In order to evaluate the expression of the angiogenesis genes (VEGF and VEGFR), chorioallantoic membranes of samples were collected and then their RNA was extracted. The amount of RNA extracted was evaluated by NanoDrop method and then RNA was used as a template for cDNA synthesis. The synthesized cDNA entered the qPCR reaction to evaluate the expression of genes associated with angiogenesis. To perform the reaction, a mixture including cDNA (1 μL), primer (2 μL), SYBR Green (10 μL), and distilled water (7 μL) was prepared and analyzed under a specific time-temperature program using a CFX-96 Bio-Rad apparatus.

Scratch Assay

For this purpose, the MCF-7 cells (5×10^5 cells/well) were cultured in 6-well plates coated with 20 μg/mL collagen. When the cell density reached 90%, a scratch was made on the bottom of the plate using a pipette tip and the cell debris was washed using PBS. Twenty-four hours after culture, the cells were exposed with a medium concentration (IC_{50}) of αT-PLC-NPs and then the cells were transferred to an incubator. At intervals of 24 and 48 h, micrographs were prepared from the scratch area in the treatment and control groups and the rate of cell migration was evaluated.

In vitro Apoptosis Assay

The effect of αT-PLC-NPs on induction of apoptosis was evaluated by different methods of staining, flow cytometry, and expression of genes related to this process.

Cell Cycle Assay

First, the 2×10^5 MCF-7 cells/well were transferred in a 6-well plate and, 24 h later, they were treated with concentrations obtained from MTT (concentrations associated with IC_{50}) assay. Forty-eight hours after treatment, the supernatant was drained and the cells were separated from the bottom of the plate with trypsin and transferred to a 1.5 mL microtube and then centrifuged. After twice washing, the supernatant of cells was removed and 400 μL of PI dye (1 mg/5 mL PBS + Triton X100)

was added to the cell sediment and, after 10 min, they were analyzed by flow cytometry analyzer (32).

AO/PI Double Staining

The MCF-7 cells (2×10^5 cells/well) were cultured on a 6-well plate and after 24 h were treated with different concentrations obtained from MTT test. Forty-eight hours later, the treatment medium of cells was drained and 1 mL of PBS solution containing 1 µL of AO (1 mg/5 mL) and 1 µL of PI (1mg/3mL) was added to each well and immediately imaged by fluorescent invert microscope.

Molecular Analysis by Real-time PCR Assay

To investigate the apoptosis signaling in αT-PLC-NPs-treated cells, the cells were first cultured on a 6-well plate and treated with various doses of αT-PLC-NPs 24 h later. After 48 h, the total RNA of the cells was extracted using the Norgen kit according to the manufacturer's protocol of and, after quantification by NanoDrop method, RNA was used as a template for cDNA synthesis. The synthesized cDNA with a specific primer, SYBR Green and DW in a total volume of 20 µL, were subjected to a real-time PCR reaction.

Antibacterial Activity Assay

Kirby-Bauer Disk Diffusion

The experiment was performed in 3 replications and used gram-positive bacteria *Staphylococcus aureus* (ATCC 25923) and *Micrococcus luteus* (ATCC 4698) and gram-negative bacteria *Escherichia coli* (ATCC 1330) and *Klebsiella pneumoniae* (ATCC 700603). With the help of a sterile swab of bacterial suspension (equivalent to half McFarland tube turbidity), was cultured uniformly on Mueller–Hinton agar medium. Disks impregnated with αT-PLC-NPs and antibiotics were placed on the environment's surface using sterile pence at standard distances. The plates were incubated at 37 ° C under aerobic conditions for 24 h. After this period, the diameter of the growth inhibition zone of each sample was measured in millimeters using a ruler. Gentamicin antibiotic disk (as a control) was used to confirm antibiotic susceptibility tests.

MIC and MBC Methods

In order to determine MIC and MBC, microbroth dilution method was used. In this method, 24-well plates were used. The αT-PLC-NPs were prepared at concentrations of 0.25, 0.5, 0.75, 1, 1.25, 1.5, 1.75, and 2 mg/mL. Chloramphenicol antibiotic powder with a concentration of 100 µg/mL was used as a control. After inoculating the bacteria in the wells, the plate was incubated at 37 ° C for 24 h. After incubation, the first well in which no growth was observed was considered MIC. From these concentrations and higher dilutions, 10 µL was transferred to nutrient agar medium; concentration in which no growth was observed was considered MBC.

In vitro Anti-inflammation Assay

The effect of αT-PLC-NPs on induction or inhibition of inflammation was evaluated by molecular analysis. For this purpose, the cells were treated with different concentrations of nanoparticles. After 48 h, their RNA was extracted and, similar to the method mentioned in "Molecular Analysis by Real-time PCR Assay," the expression of inflammation-related genes was evaluated using specific primers. The sequence of primers used in this study is given in Table I.

Statistical Analysis

Statistical data analyses were done on all results by a one-way ANOVA followed by LSD test with $p < 0.05$ as the minimal significance level.

RESULTS

Characterization of αT-PLC-NPs

Particle size, zeta potential, and their stability are significantly related to the mass ratio of phospholipids to chitosan (25). Studies have shown that nanoparticles synthesized with a mass ratio of phospholipid to chitosan in the range 5:1–20:1 have a small size (below 280 nm), narrow size distribution, strong positive potential, and high stability (25). DLS results of αT-PLC-NPs with a mass ratio of phospholipid to chitosan 1:15 showed the formation of spherical nanoparticles with dimensions of 220.8±4.36 nm, PDI of 0.3±0.02, and surface charge of +29.03±17.9 mV (Fig. 1A). In FTIR spectrum of αT-PLC-NPs (Fig. 1), the characteristic peaks of α-T, chitosan, lecithin, and PEG were found to be shifted slightly, which confirms the interaction between the compounds used in nanoparticle synthesis and formation of αT-PLC-NPs. The characteristic peaks of lecithin in the FTIR spectrum are a peak at 3379 cm^{-1} (N–H group stretching) (33), 3009 cm^{-1} (cis-double bond), 1735 cm^{-1} (saturated aliphatic ester carbonyl stretching) (34), 2923 cm^{-1} and 2853 cm^{-1} (C–H stretching vibration of methylene group), 1735 cm^{-1})C=O stretching vibration(, 1465 cm^{-1} (C–H bending vibration of methyl group), 1240 cm^{-1} (P=O stretching vibration), and 1062 cm^{-1} (P–O–C stretching vibration) (35). PEG characteristic absorption bands have been as follows: a peak at 840 cm^{-1} (C–O, C–C stretching, CH2), 960 cm^{-1} (CH$_2$ rocking, CH$_2$ twisting), 1058 cm^{-1} (CH$_2$ rocking), 1145 cm^{-1} (C–O stretching, CH$_2$ rocking), 1241 and 1278 cm^{-1} (CH$_2$ twisting), 1341 cm^{-1} (CH$_2$ wagging), and 1466 cm^{-1} (CH$_2$ scissoring) (36). Chitosan characteristic absorption bands have been as follows: a peak at 3354 cm^{-1} and 3291 cm^{-1} (NH2 stretching vibration), 1651 cm^{-1} and 1585 cm^{-1} (N–H bending of primary amine), 1199 cm^{-1} and 1150 cm^{-1} (C–O stretching of C–O–C), two peaks at 1058 cm^{-1} and 1026 cm^{-1} (primary aliphatic amine stretching of C–N overlapping with secondary cyclic alcohol stretching of O–H), and a peak at 894 cm^{-1} (pyranoid ring of chitosan) (37). α-T characteristic absorption bands have been as follows: the absorption band at 3393 cm^{-1} (N–H, O–H), 2923 cm^{-1} (C–H stretch), 1659 cm^{-1} (C=C, C=C-H), 1444 cm^{-1} (C=C, aromatic), and 1156 cm^{-1} (C–O stretch) (38). FESEM and TEM image of αT-PLC-NPs (Fig. 1C, D) shows spherical nanostructures

Table I Sequence of Primers

Gene	Forward	Reverse
GAPDH	TGCTGGTGCTGAGTATGTCG	GCATGTCAGATCCACAACGG
P53	ACA CGC TTC CCT GGA TTG G	GGT CTT GGC CAG TTG GCA A
P21	AAGACCATGTGGACCTGTCACTGT	GAAGATCAGCCGGCGTTTG
CAS 9	CCAGAGATTCGCAAACCAGAGG	GAGCACCGACATCACCAAATCC
TNF-α	CAG AGG GAA GAG TTC CCC AG	CCT TGG TCT GGT AGG AGA CG
IL-6	CAAATTCGGTACATCCTC	CTGGCTTGTTCCTCACTA
Actin	AGACAGCTACGTTGGTGATGAA	TGCTCCTCAGGGGCTACTCT
VEGF	GACCTGTAAATGTTCCTGCAA	AGAAATCAGGCTCCAGAAACA
VEGFR-2	TCACGCCTTACAGACACCCT	AGGGAGATGTTACGGAGAATG

with diameters below 100 nm, which is consistent with the results of DLS. In this study, in order to evaluate the stability of αT-PLC-NPs, the physicochemical properties of nanoparticles were evaluated after 4 months of storage at 2–8 °C and the results showed the presence of nanoparticles with a size of 255.5 nm, dispersion index of 0.28, and zeta potential of 22.43 mV. The results show that during storage, slight changes were made in the studied indices, which includes an increase in the size of nanoparticles and a decrease in their dispersion and surface charge index (Fig. 1A).

Entrapment Efficiency and Release of α-T

The amount α-T encapsulated in PLC-NPs was determined by indirect method (39–41). By comparing the level below the peak of the supernatant obtained from a synthesis process (Fig. 2B) with the standard of α-T (Fig. 2A) and considering the volume of supernatant and the initial amount of α-T used in the reaction, it was determined that 16.5 mg of α-T has been released. Due to the density of αT (934 mg/mL) and the substitution of numbers in the corresponding
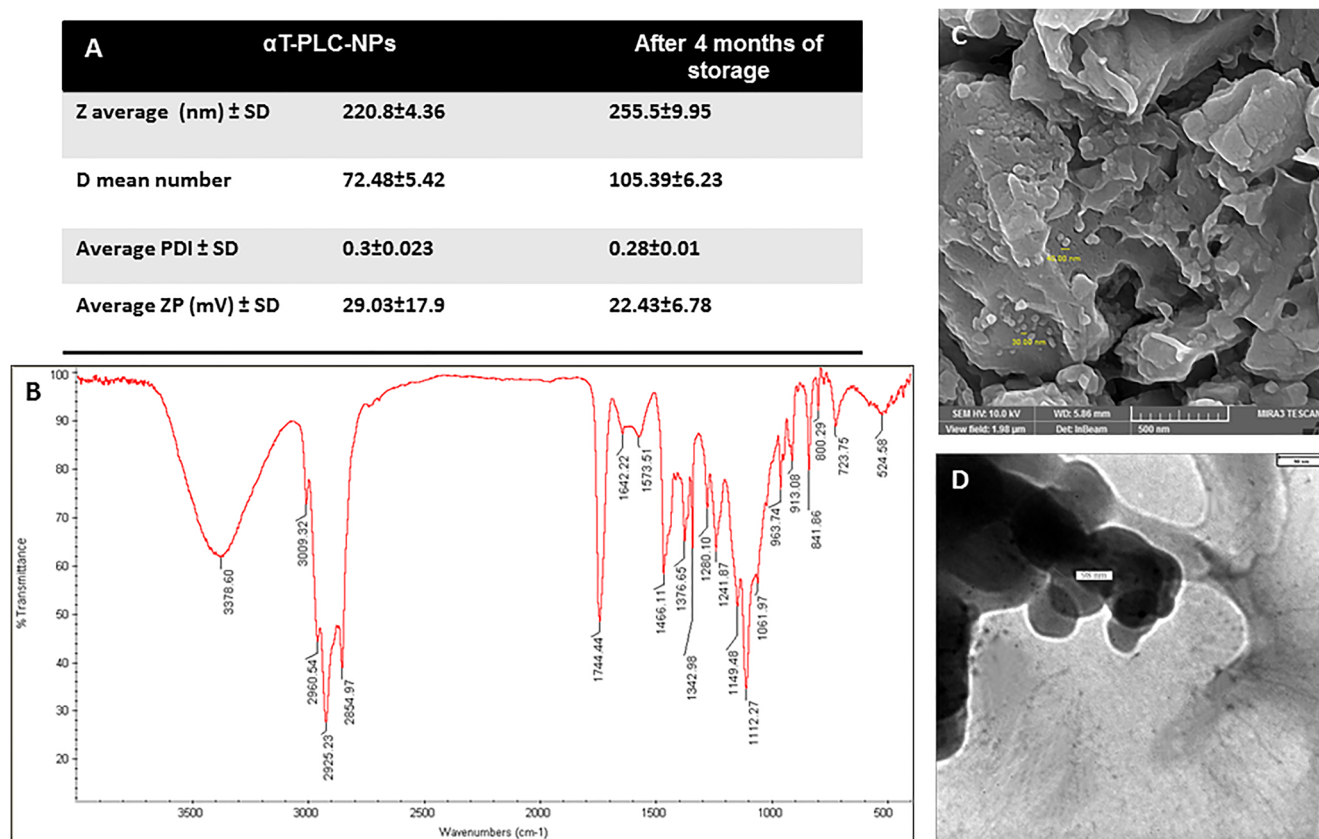

A	αT-PLC-NPs	After 4 months of storage
Z average (nm) ± SD	220.8±4.36	255.5±9.95
D mean number	72.48±5.42	105.39±6.23
Average PDI ± SD	0.3±0.023	0.28±0.01
Average ZP (mV) ± SD	29.03±17.9	22.43±6.78

Fig. 1 Characterization data. **A** Physicochemical properties of αT-PLC-NPs at the beginning of synthesis and after 4 months of storage. **B** FTIR spectra of αT-PLC-NPs. **C**, **D** FESEM and TEM images of αT-PLC-NPs

formula, the encapsulation efficiency was reported to be 82 ± 3.1%. The cumulative release curve of α-T from αT-PLC-NPs is shown in Fig. 2C. As shown in the diagram, α-T's release was slow and without explosive effect. The emission rate in the first 48 h was reported to be about 65%, and during the 72 and 96 h, the emission process increased slowly and reached about 68%.

Cytotoxic Effects of α-T, PLC-NPs, and αT-PLC-NPs

The toxicity effect of different concentrations of α-T on cancer cells was evaluated in comparison with normal by MTT method. The results of this study showed that α-T in a concentration of 1 mg/mL inhibited 38% of cancer cells and 18% of normal cells. The median concentration (IC_{50}) of α-T in MCF-7 cells is above 1000 μg/mL (Fig. 3A).

Blank nanoparticles (PLC-NPs) were used to investigate the possible effects of nanocarriers on the inhibition of cancer cells. The results of this study showed that PLC-NPs have no toxic effect on MCF-7 cells. Therefore, inhibition of cancer cells by αT-PLC-NPs is simply due to the presence of α-T capsulated in nanoparticles (Fig. 3B).

The morphological alterations of MCF-7 cells treated with αT-PLC-NPs compared to the control were examined using an inverted microscope. Changes in the morphology of cells from elongated to spherical, cell fragmentation, and reduction in number are among the changes in treated cells, which are shown in Fig. 3C. The results exhibited dose-dependent inhibitory effects of αT-PLC-NPs against MCF-7 cells with IC_{50} about 750 μg/mL while no toxicity was observed on HFF at similar concentrations, indicating the selective inhibitory effect of αT-PLC-NPs against cancer cells (Fig. 3D). The results of MTT test showed a higher toxicity effect of α-T capsulated in nanoparticles compared to free α-T.

ABTS and DPPH Scavenging Assay

The concentration-dependent inhibitory effect of α-T and αT-PLC-NPs on ABTS and DPPH free radicals is shown in Fig. 4. As the diagram shows, α-T has a low inhibitory effect on ABTS and DPPH free radicals. Inhibition of DPPH free radicals at a concentration of 1000 μg/mL of α-T was reported to be about 19% while in similar concentrations, about 23% of ABTS free radicals were inhibited (Fig. 4A). Also, the inhibitory effect of αT-PLC-NPs on ABTS free radicals with an average concentration of 970 μg/mL is shown in Fig. 4B. The median concentration of αT-PLC-NPs against DPPH free radicals was reported to be about 1000 μg/mL (Fig. 4C). The median concentration of glutathione against both free radicals was reported to be less than 30 μg/mL. Comparison of the median concentration of glutathione with αT-PLC-NPs on free radical scavenging shows the moderate antioxidant power of αT-PLC-NPs. The results of this study show an increase in the inhibitory power of α-T encapsulated in nanoparticles against free radicals compared to free α-T.
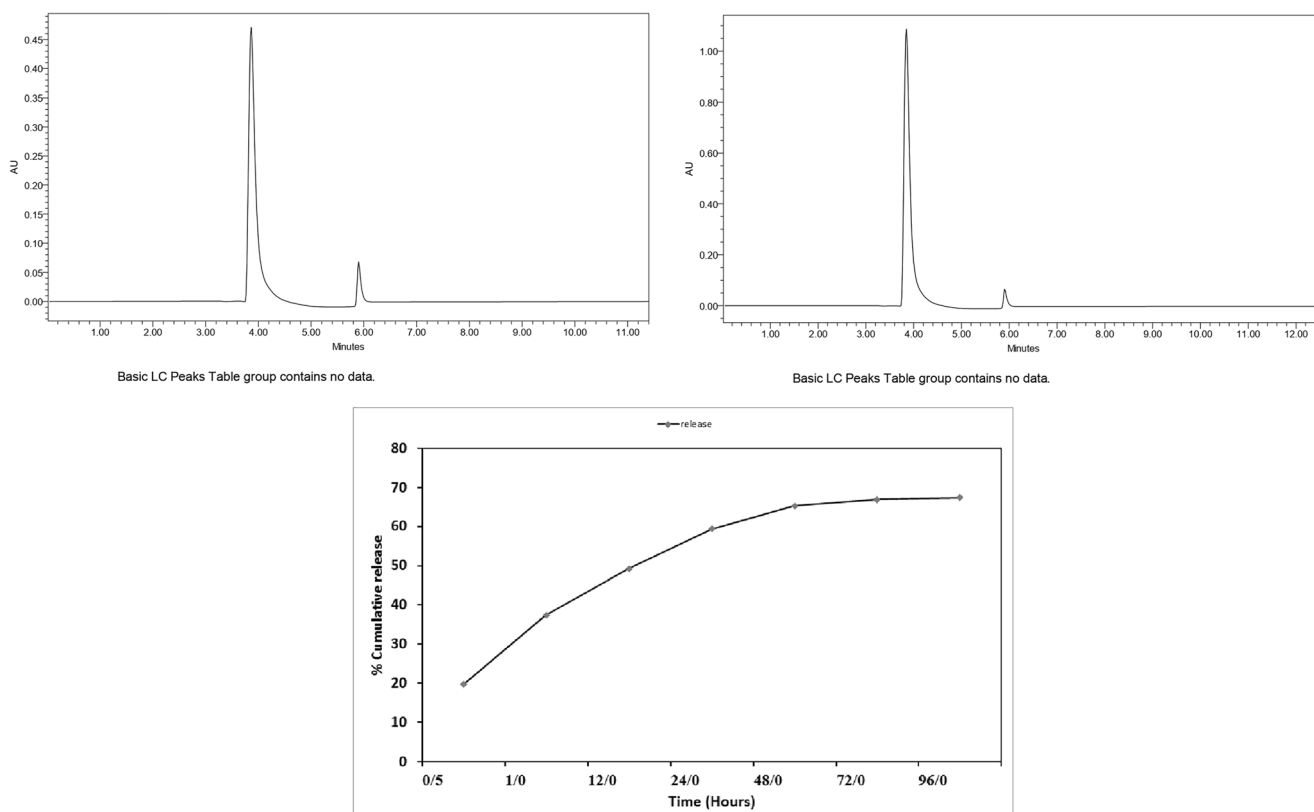

Basic LC Peaks Table group contains no data.

Basic LC Peaks Table group contains no data.

Fig. 2 α-T encapsulation and release rate. **A** HPLC chromatogram of α-T standard solution. **B** HPLC chromatogram of α-T in supernatant solution. **C** The release profiles of α-T from αT-PLC-NPs during 96 h
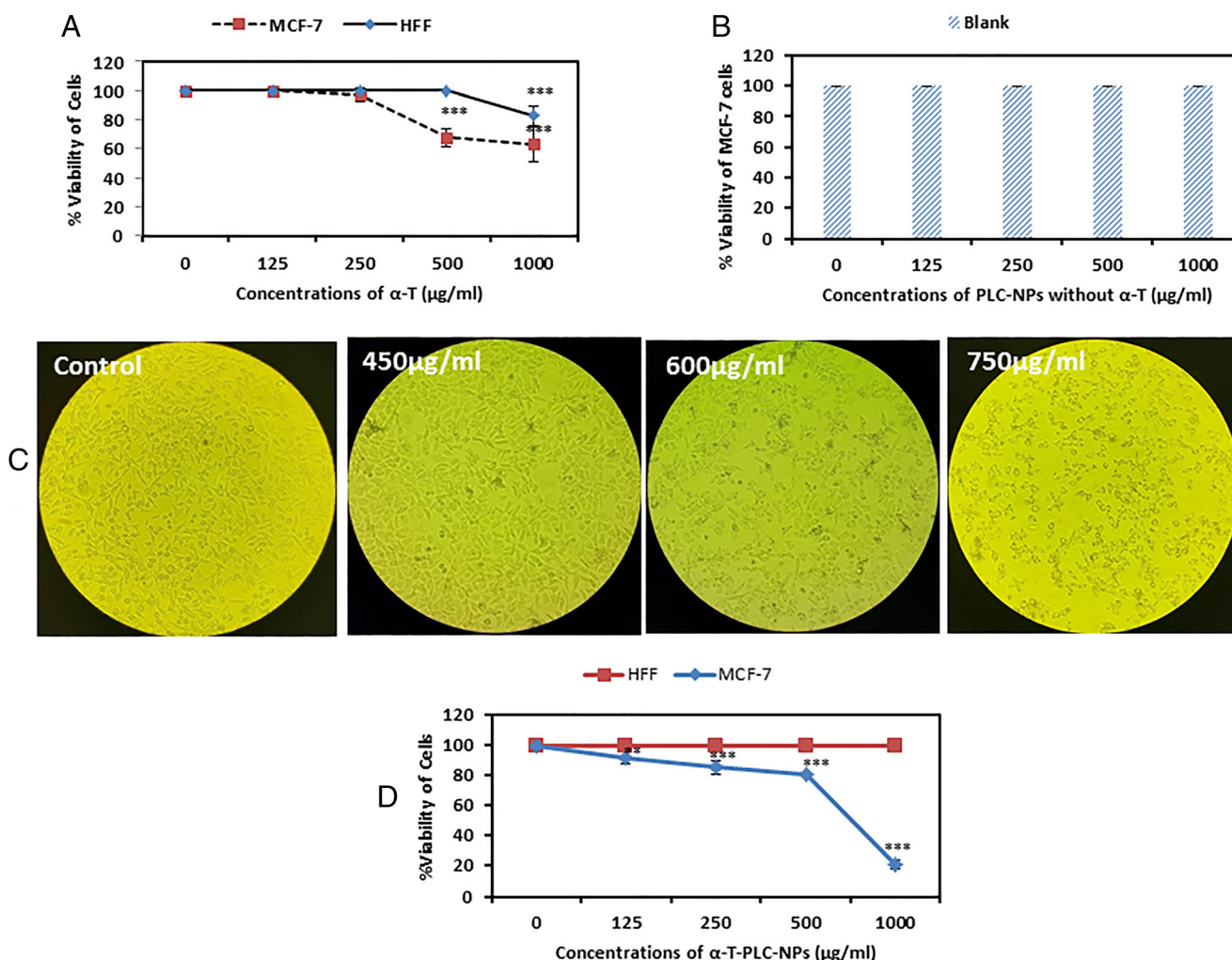
Fig. 3 MTT assay for assessment of cytotoxic effects of αT, PLC-NPs, and αT-PLC-NPs after 48-h treatment. **A** Cytotoxic effects of α-T against MCF7 and HFF cells. **B** Cytotoxic effects of blank PLC-NPs without α-T against MCF7 cells. **C** Morphological images of αT-PLC-NPs-treated MCF-7 cells compared to untreated cells. **D** The MTT diagram that shows the effect of αT-PLC-NPs treatment on HFF and MCF-7 cells. Results presented as mean ± SD; **$P<0.01$ and ***$P<0.001$ were considered significant

CAM and qPCR Assay

Imaging results of angiogenesis changes during treatment show a significant decrease in angiogenesis with increasing treatment concentration in experimental groups compared to controls (Fig. 5A). The mean number of blood vessels (29.21 ± 1.9 mm) in control samples with laboratory control (28.65 ± 2.9 mm) did not show a statistically significant difference. In addition, in the treated group with a concentration of 500 μg/mL (25.22 ± 2.2 mm), the difference was not significant compared to the control group ($P> 0.05$). By increasing the concentration to 1 mg/mL (19.1 ± 0.8 mm) and 2 mg/mL (17.68 ± 2.5 mm), a significant decrease (***$P<0.001$) was observed in the number of blood vessels compared to the control. Comparison of mean blood vessel length in control (29.21 ± 1.9 mm) and laboratory control (28.65 ± 2.9 mm) groups did not show a significant difference, while in all three experimental groups treated with αT-PLC-NPs, a significant and concentration-dependent reduction in blood vessel length was reported compared to control (*$P<0.05$ and ***$P<0.001$). Evaluation of changes in embryo length and weight in samples treated with

αT-PLC-NPs compared to the control group showed a significant reduction (*$P<0.05$ and **$P<0.01$) in samples treated with concentrations of 1 and 2 mg/mL (Fig. 5B). Downregulation of VEGF and VEGF-R genes in chorioallantoic membranes extracted from the treated samples compared to the control sample indicates the inhibitory effect of αT-PLC-NPs on the angiogenesis signaling at the molecular level. Since VEGF and VEGF-R genes are known as the most important genes involved in angiogenesis, inhibition of these genes can have an effective role in reducing angiogenesis and blood flow to tumor tissue (Fig. 5C).

Scratch Assay

Considering that the migration of cancer cells plays an important role in the onset of metastasis and tumor progression to other parts of the body, in this study, the migration of breast cancer cells treated with nanoparticles was investigated *in vitro* and the results showed that after 24 and 48 h of incubation in the sample witnessed cell migration to the scratch area is about 58.63% and 100%, while in the sample
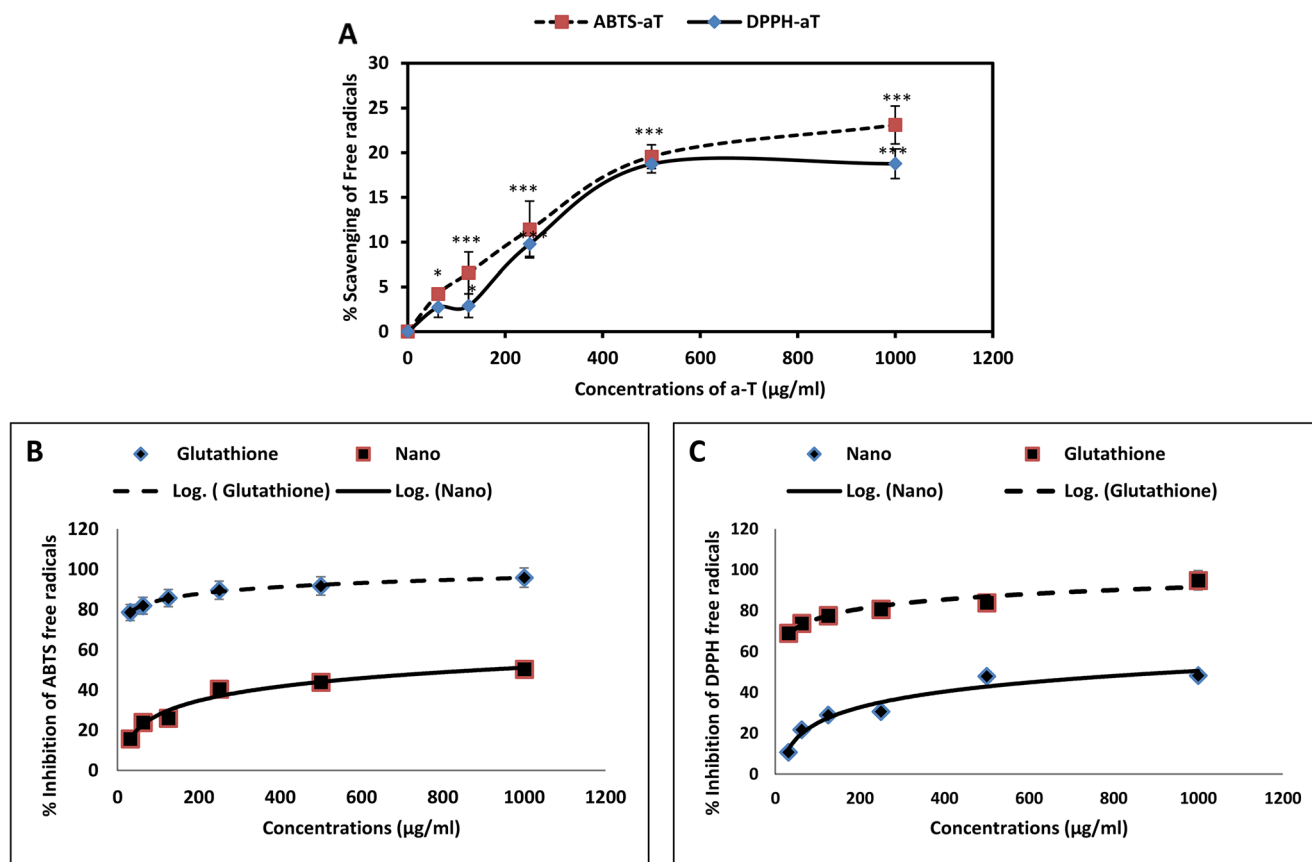
Fig. 4 ABTS and DPPH free radical scavenging assay. **A** α-T free radical scavenging capacity. **B** Inhibitory effect of αT-PLC-NPs on the scavenging of ABTS free radicals. **C** Inhibitory effect of αT-PLC-NPs on the scavenging of DPPH free radicals. Results presented as mean ± SD; *$P<0.05$ and ***$P<0.001$ were considered significant

treated with nanoparticles, about 91% of cell migration to the scratch area was prevented. These results demonstrate the effects of αT-PLC-NPs in inhibiting cell migration and preventing metastasis and tumor progression in breast cancer (Fig. 6).

Apoptosis Assay

Cell cycle analysis showed that in the control sample less than 1% of the cells are in the SubG1 phase, and about 99% of the cells have entered the next stages of the cell cycle, while in the treated samples, with increasing treatment concentration from 450 to 600 and 750 μg/mL, the percentage of SubG1 phase cells increased from 10.1 to 19.9 and 64.5%, respectively. At 450 μg/mL concentration, cell arrest was shown in addition to the SubG1 in the G2-M phase. Cell arrest in different phases of the cell cycle confirms the pro-apoptotic effects of αT-PLC-NPs on MCF-7 cells (Fig. 7A).

Figure 7B shows changes in the nucleus and cytoplasm of nanoparticle-treated cancer cells compared to untreated cells in the form of discoloration emitted from the cell. Acridine dye is a vital dye that makes healthy cells green, while PI dye is able to penetrate damaged cells and emit red dye. As can be seen in the control samples, all cells are green and have an elongated morphology. While in cells treated with two concentrations of 450 and 600 μg/mL, apoptotic changes such as cytoplasmic germination, cell rounding, swelling, increase in size, and decrease in cell number are observed. In treated

cells with a concentration of 750 μg/mL, PI dye penetration and an increase in apoptotic cells (red) are observed.

P53 is one of the effective factors in the occurrence of apoptosis in cells. This factor causes apoptosis in cells by activating proteins involved in the extrinsic apoptosis pathway, endoplasmic reticulum proteins and caspases, including caspase-9. In fact, p53 protein stimulates apoptosis in tumor cells at the transcriptional level by increasing and decreasing the effect on pro-apoptotic and anti-apoptotic genes (42, 43). P21 is a downstream target of p53 and a cell cycle inhibitor (44). Figure 7C shows the increase in the expression of p53, p21, and caspase 9 genes in αT-PLC-NPs-treated cells (dose-dependently) compared to controls.

Antibacterial Effects of αT-PLC-NPs

Figure 8 A and B show the average growth inhibition zone (IZ) for different bacterial strains exposed to αT-PLC-NPs. The results of this study show that *Escherichia coli* (IZ: 0) as a gram-positive bacteria has the highest resistance to treatment while *Staphylococcus aureus* (IZ: 18mm) as a gram-negative bacteria is the most sensitive strain to treatment among the studied strains. Gentamicin showed a growth inhibition zone with an average of about 21 mm in all four bacterial strains. Calculation of MIC and MBC values in samples treated with different concentrations of αT-PLC-NPs showed the highest sensitivity for *Staphylococcus aureus* samples at a minimum inhibitory concentration of 0.5
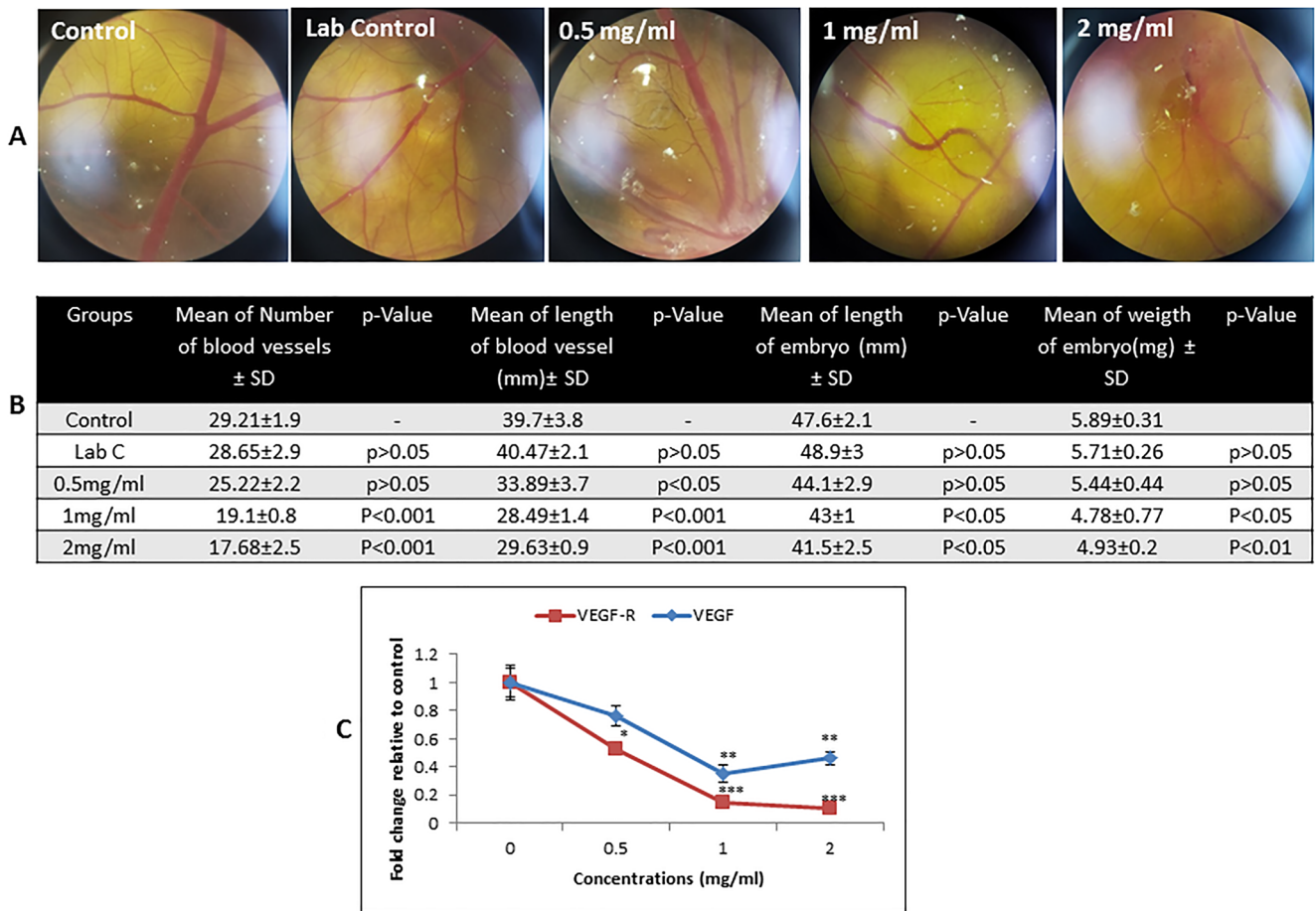
Groups	Mean of Number of blood vessels ± SD	p-Value	Mean of length of blood vessel (mm)± SD	p-Value	Mean of length of embryo (mm) ± SD	p-Value	Mean of weigth of embryo(mg) ± SD	p-Value
Control	29.21±1.9	-	39.7±3.8	-	47.6±2.1	-	5.89±0.31	
Lab C	28.65±2.9	p>0.05	40.47±2.1	p>0.05	48.9±3	p>0.05	5.71±0.26	p>0.05
0.5mg/ml	25.22±2.2	p>0.05	33.89±3.7	p<0.05	44.1±2.9	p>0.05	5.44±0.44	p>0.05
1mg/ml	19.1±0.8	P<0.001	28.49±1.4	P<0.001	43±1	P<0.05	4.78±0.77	P<0.05
2mg/ml	17.68±2.5	P<0.001	29.63±0.9	P<0.001	41.5±2.5	P<0.05	4.93±0.2	P<0.01

Fig. 5 CAM and qPCR assay to evaluate the anti-angiogenesis effects of αT-PLC-NPs. **A** Reduction of blood vessels in stereomicroscopic images in control and αT-PLC-NPs-treated samples. **B** Reduction in the number and length of blood vessels as well as embryonic growth factors in samples treated with different doses of αT-PLC-NPs compared to the control. **C** Decreased expression of VEGF and VEGFR genes in the chorioallantoic membrane extracted from treated samples compared to control samples. All data were presented as mean±SD
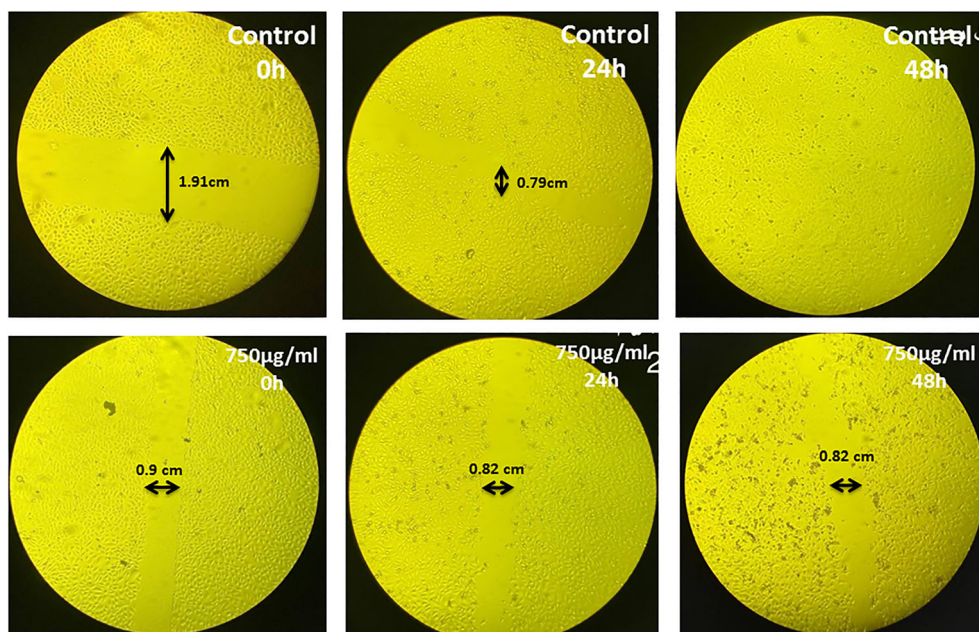

Fig. 6 MCF-7 cell migration assay during 48 h of treatment with 750 μg/mL αT-PLC-NPs
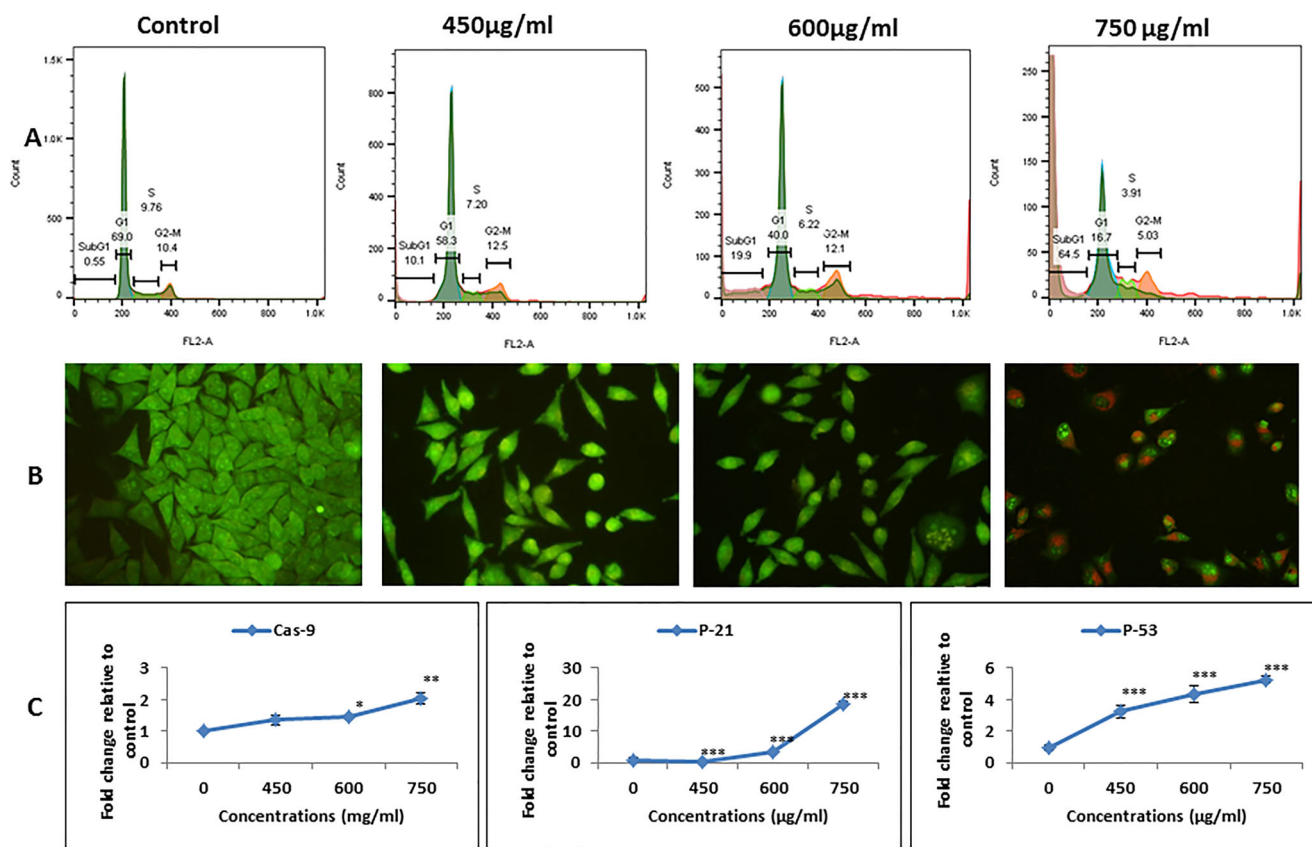
Fig. 7 Apoptosis assay. **A** Flow cytometry assay. **B** AO/PI staining. **C** Gene expression assay (*P<0.05, **P<0.01, and ***P <0.001) in αT-PLC-NPs-treated cells compared to untreated cells

(Fig. 8C) and a minimum lethal concentration of 1.25 µg/mL (Fig. 8D).

Anti-inflammation Assay

TNF-α and IL-6 are among the pro-inflammatory cytokines that increase in diseases such as cancer. Decreased expression of these genes can lead to reduced inflammation and side effects (45). Examination of TNF-α gene expression showed that in treated cells with concentrations of 600 and 750 µg/mL αT-PLC-NPs, the expression of this gene is reduced by about 20 and 49%. Significant reduction (above 80%) in interleukin 6 gene expression was also confirmed by treatment with αT-PLC-NPs by qPCR method.

DISCUSSION

In this study, α-T loaded on PLC-NPs were successfully synthesized by solvent-injection method with high encapsulation efficiency (82%) and analyzed for physicochemical properties, and antioxidant, anti-cancer, anti-inflammation, and antibacterial effects in *in vitro* and *in vivo* models. The use of lecithin (phosphatidylcholine) due to its safety and high biocompatibility and the possibility of loading hydrophobic drugs in the synthesis of various nanocarriers including micelles, liposomes, and lipid nanoparticles have been reported in previous studies (35, 46). Coating this structure with natural polymers such as chitosan through the formation of supramolecular self-assembly causes the formation of stable, biocompatible, and biodegradable

nanostructures with excellent mucosal adhesion and minimal cytotoxicity and can play an effective role in increasing the efficiency of the formulation (47). There are several methods for synthesizing lecithin/chitosan nanoparticles, such as spray drying, emulsion crosslinking, ion coagulation, and solvent injection (48). In this study, similar to some previous studies (18, 46), solvent injection procedure was used as an easy and widely used method.

Modification of nanoparticles according to their type is a suitable approach to trap and suppress the side effects of drugs and can reduce the effective dose and adverse symptoms of the drug by increasing the concentration of the drug in the target organs or tissues (49). In some studies, various methods have been used to modify LC-NPs to improve their performance. For instance, in a 2010 study, isopropyl myristate was added to the ethanol phase to improve the distribution of clobetasol propionate in the lipid nucleus and increase its encapsulation efficiency (50). In another study in 2018 (51) similar to the present study, PEG bonding was used to modify the surface of lecithin-chitosan nanoparticles. Surface modification of LC-NPs with PEG can increase the loading efficiency, improve the bioavailability, increase the half-life of the drug, reduce the release efficiency, and reduce the removal by the reticuloendothelial system (RES) (37).

Loading of αT in PLC-NPs resulted in the formation of nanoparticles with dimensions of 220.8 nm, PDI of 0.3, and surface charge of +29.03 mV with an encapsulation efficiency of 82%. Various studies have investigated the efficiency of
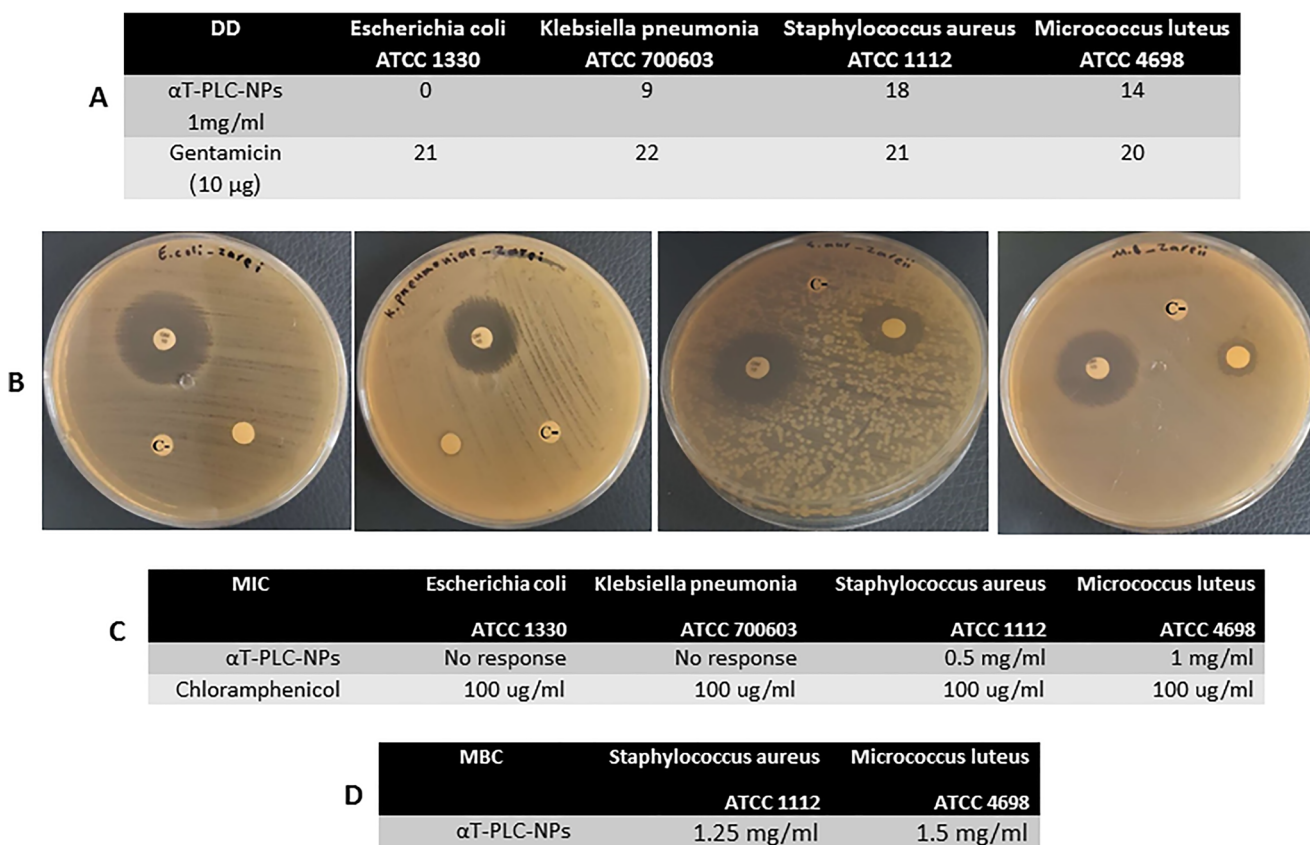
	DD	Escherichia coli ATCC 1330	Klebsiella pneumonia ATCC 700603	Staphylococcus aureus ATCC 1112	Micrococcus luteus ATCC 4698
A	αT-PLC-NPs 1mg/ml	0	9	18	14
	Gentamicin (10 μg)	21	22	21	20

	MIC	Escherichia coli ATCC 1330	Klebsiella pneumonia ATCC 700603	Staphylococcus aureus ATCC 1112	Micrococcus luteus ATCC 4698
C	αT-PLC-NPs	No response	No response	0.5 mg/ml	1 mg/ml
	Chloramphenicol	100 ug/ml	100 ug/ml	100 ug/ml	100 ug/ml

	MBC	Staphylococcus aureus ATCC 1112	Micrococcus luteus ATCC 4698
D	αT-PLC-NPs	1.25 mg/ml	1.5 mg/ml

Fig. 8 Antibacterial assay. **A**, **B** Comparison of the growth inhibition zone of bacterial strains (*Escherichia coli*, *Micrococcus luteus*, *Klebsiella pneumonia*, and *Staphylococcus aureus*) exposed with αT-PLC-NPs compared to gentamicin as a standard antibiotic, **C** MIC assay, **D** MBC assay.

LC-NPs in drug delivery using different models and the results of these studies have shown that the encapsulation efficiency of hydrophobic molecules in these nanocarriers is high, while hydrophilic molecules are less loaded in these nanostructures (25, 47). In one study, tamoxifen citrate was used to load LC-NPs and the optimal formulation led to particle formation with size of 94.8 nm and % EE of 81.3% (52) that compared to αT-PLC-NPs, it shows smaller size and similar encapsulation efficiency. In a study in 2019, the loading of cisplatin in LC-NPs resulted in the formation of nanoparticles with a diameter of 181 nm and a loading percentage of 89.2% (21), which compared to the present study shows smaller diameter and higher loading efficiency. The loading efficiency of melatonin (53) and β-lapachone (54) in LC-NPs with diameters of 122.8 and 330.1 nm was reported to be 7.1 and 52.4 %, respectively, which shows a lower loading rate compared to the present study.

Bioactive compounds with antioxidant potential play a key role in preventing the growth of cancer cells (55). The ability of α-T to inhibit free radicals *in vitro* has been investigated and confirmed in a study at 2014 (56). Evaluation of antioxidant power of αT-PLC-NPs confirmed its inhibitory effect on free radicals *in vitro*. Figure 4 shows the higher power of αT-PLC-NPs for hydrogen donation to stabilize ABTS free radicals compared to DPPH. Similarly, in a 2014 study, the inhibitory potency of quercetin-loaded lecithin/chitosan nanoparticles against DPPH free radicals was reported (57). Also, in another study in 2021, the inhibitory

effect of Tmx-Cu-LPHNPs on ABTS and DPPH free radicals with moderate concentrations of 998.125 and 164.87 μg/mL was reported (58), which is comparable to the present study.

The use of natural compounds with antibacterial effects can play an effective role in reducing bacterial infections and, consequently, preventing inflammatory diseases such as cancer (59). The antibacterial effects of α-T have been confirmed in previous studies (15, 56). In the present study, lipid-polymer nanocarriers were used to transfer and evaluate the toxicity of α-T on bacterial cells. LC-NPs are thermodynamically suitable for fusion with lipid membranes due to positive surface charge, and this fusion increases with electrostatic adsorption between the cationic charge of the nanoparticles and the anionic charge in the pathogen, leading to lysis of pathogenic cells (60). The ability of αT-PLC-NPs to inhibit the growth of *Staphylococcus aureus* and *Micrococcus luteus* as gram-positive bacteria was confirmed in this study.

Inflammation is an essential response of the immune system to fight infections. Pro-inflammatory cytokines play a major role in causing inflammation. However, excessive increase of pro-inflammatory factors and their uncontrolled production can cause chronic inflammatory conditions and related diseases such as osteoarthritis and cancer (61). Due to the fact that chronic inflammation in diseases such as cancer is associated with side effects, reducing some of the pro-inflammatory factors such as TNF-α, IL-6, and IL-1β can help manage cancer treatment and reduce its complications (45). α-T has been shown to possess anti-inflammatory properties by reducing the
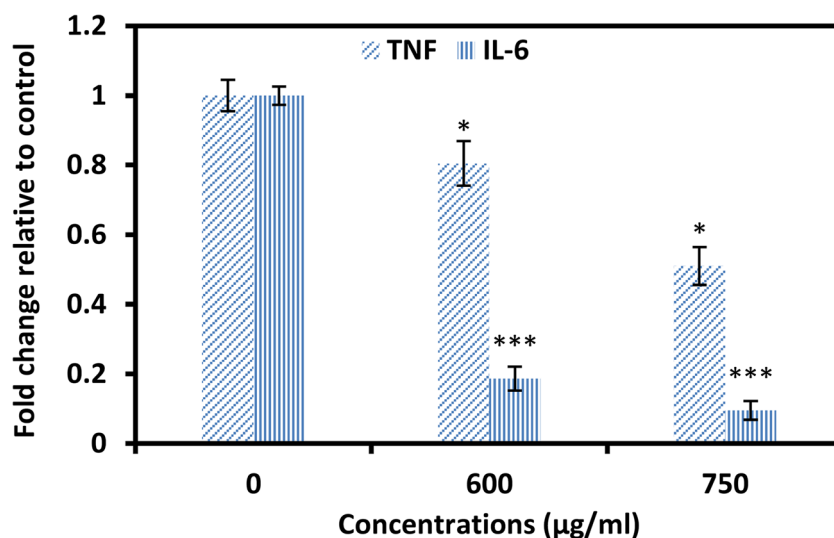
Fig. 9 Inflammatory gene expression assay (*$P<0.05$ and ***$P <0.001$) in αT-PLC-NPs-treated cells compared to untreated cells (N=3)

levels of several pro-inflammatory cytokines (TNF-α, IL-6, IL1R1, and IL-1β) (62). In the current study, the inhibitory effect of αT-PLC-NPs on TNF-α and IL-6 as pro-inflammatory cytokines was confirmed by qPCR way (Fig. 9).

The nanometer size and positive surface charge of LC-NPs make it a suitable carrier for drug delivery to cancer cells. Positively charged chitosan coating on the nanoparticle surface can bind to negatively charged cancer cells and facilitate drug delivery in the acidic environment of the tumor (1). In the present study, the MTT results showed that αT-PLC-NPs are able to inhibit MCF-7 cells (IC$_{50}$: 750 μg/mL) with higher potency compared to HFF as normal cells (IC$_{50}$: about 1000 μg/mL). In a study conducted in 2021, the toxicity of LC-NPs containing tamoxifen and curcumin against different cell lines was investigated. The IC$_{50}$ value was reported to be less than 100 μg/mL for all cancer cell lines that were studied (58). The higher cytotoxic effect of Tmx-Cu-LPHNPs is probably related to the simultaneous loading of the two compounds (Tmx-Cu) and their synergistic effect. Valencia *et al.* (2021) examined the cytotoxicity of curcumin-loaded LC-NPS (Ps: 236.27 nm, PDI: 0.1, ζ P: +51.31 and EE: 92.74%) in HCT-116 and NCI-H292 cells. NPC showed no cytotoxicity against normal cells while inhibited cancer cells with IC$_{50}$ about 70 μg/mL (31). The cytostatic (arrest of G0/G1 phase) and cytotoxic (by induction of apoptosis) effects of α-T have been confirmed in previous studies. The selective toxicity of α-T against malignant lymphocytes compared to normal lymphocytes was reported in a study by Lindhagen *et al.* This feature is an advantage for α-T because other clinical cytotoxic drugs are unable to select cytotoxicity between malignant and normal lymphocytes (12). In addition, cell cycle arrest and apoptosis in malignant lymphocyte cells were reported in a dose- and time-dependent manner in α-T therapy. Similar results were reported in confirming the inhibitory effects of α-T on the cell cycle and its pro-apoptotic effects in another study by Itani *et al.* (63). In the present study, the effects of α-T loaded on PLC-NPs on apoptosis induction were confirmed by inhibiting cell cycle in SubG1 phase, increasing apoptosis-promoting genes and AO/PI staining which are similar to the results of a study in 2021. In this study, cell cycle arrest in SubG1 phase, increase in caspase 9 and p53 genes

and AO/PI results confirmed the pro-apoptotic effects of Tmx-Cu-LPHNPs (58).

The formation of new blood vessels and blood supply to tumor tissue play an important role in the growth and development of tumors, and inhibition of blood flow can effectively prevent tumor growth (8). In tumor vessels, the distance between the endothelial cells lining the vessels is about 100 to 780 nm (9, 64), which allows the transfer of drug compounds with the help of nanocarriers. On the other hand, drainage of the tumor lymphatic network is not enough, so drugs that leak into the middle part of the tumor remain there for a long time, and this feature is known as the EPR effect, which causes the drug to accumulate in the tumor microenvironment (65). In this study, for the first time, the inhibitory effects of αT-PLC-NPs on angiogenesis were investigated and confirmed by various methods. In previous studies, the inhibitory role of chitosan nanoparticles loaded with bioactive compounds or drugs on angiogenesis has been reported (66–68), which is comparable to the present study.

CONCLUSION

The results of this study showed the presence of uniform particles with dimensions of 220.8 nm and high stability that can inhibit breast cancer cells by stopping the cell cycle, inducing the intrinsic apoptosis pathway and inhibiting angiogenesis. Due to the antioxidant, antibacterial, and anti-cancer properties of αT-PLC-NPs, the use of these nanoparticles in cancer therapy studies is recommended.

AUTHOR CONTRIBUTION

Masoud Homayouni Tabrizi conceived of the presented idea. Bahar Zarei, Masoud Homayouni Tabrizi, and Amir Rahmati performed the experiments and computations.

FUNDING

DECLARATIONS

Conflict of Interest The authors declare no competing interests.

REFERENCES

1. Abbasi N, Homayouni Tabrizi M, Ardalan T, Roumi S. Cerium oxide nanoparticles-loaded on chitosan for the investigation of anticancer properties. Materials Technology. 2021:1–11.
2. Dai X, Xiang L, Li T, Bai Z. Cancer hallmarks, biomarkers and breast cancer molecular subtypes. Journal of Cancer. 2016;7(10):1281–94.
3. Gorrini C, Baniasadi PS, Harris IS, Silvester J, Inoue S, Snow B, Joshi PA, Wakeham A, Molyneux SD, Martin B, Bouwman P, Cescon DW, Elia AJ, Winterton-Perks Z, Cruickshank J, Brenner D, Tseng A, Musgrave M, Berman HK, et al. BRCA1 interacts with Nrf2 to regulate antioxidant signaling and cell survival. Journal of Experimental Medicine. 2013;210(8):1529–44.
4. Asadi-Samani M, Farkhad NK, Mahmoudian-Sani MR, Shirzad H. Antioxidants as a double-edged sword in the treatment of cancer. IntechOpen: Antioxidants; 2019.
5. Soltani M, Etminan A, Rahmati A, Behjati Moghadam M, Ghaderi Segonbad G, Homayouni TM. Incorporation of Boswellia sacra essential oil into chitosan/TPP nanoparticles towards improved therapeutic efficiency. Materials Technology. 2021:1–13.
6. Van Loenhout J, Peeters M, Bogaerts A, Smits E, Deben C. Oxidative stress-inducing anticancer therapies: taking a closer look at their immunomodulating effects. Antioxidants. 2020;9(12):1188.
7. Fulda S, Debatin K-M. Extrinsic versus intrinsic apoptosis pathways in anticancer chemotherapy. Oncogene. 2006;25(34):4798–811.
8. Teleanu RI, Chircov C, Grumezescu AM, Teleanu DM. Tumor angiogenesis and anti-angiogenic strategies for cancer treatment. Journal of Clinical Medicine. 2020;9(1):84.
9. Shabestarian H, Homayouni Tabrizi M, Movahedi M, Neamati A, Sharifnia F. Putative mechanism for cancer suppression by PLGA nanoparticles loaded with Peganum harmala smoke extract. Journal of Microencapsulation. 2021;38(5):324–37.
10. Yan L, Shen J, Wang J, Yang X, Dong S, Lu S. Nanoparticle-based drug delivery system: a patient-friendly chemotherapy for oncology. Dose-Response. 2020;18(3):1559325820936161.
11. Moon JH, Moxley JW Jr, Zhang P, Cui H. Nanoparticle approaches to combating drug resistance. Future Medicinal Chemistry. 2015;7(12):1503–10.
12. Hassan SB, Gali-Muhtasib H, Göransson H, Larsson R. Alpha terpineol: a potential anticancer agent which acts through suppressing NF-κB signalling. Anticancer Research. 2010;30(6):1911–9.
13. Held S, Schieberle P, Somoza V. Characterization of α-terpineol as an anti-inflammatory component of orange juice by in vitro studies using oral buccal cells. Journal of Agricultural and Food Chemistry. 2007;55(20):8040–6.
14. Bicas J, Neri-Numa I, Ruiz A, De Carvalho J, Pastore G. Evaluation of the antioxidant and antiproliferative potential of bioflavors. Food and Chemical Toxicology. 2011;49(7):1610–5.
15. Li L, Shi C, Yin Z, Jia R, Peng L, Kang S, Li Z. Antibacterial activity of α-terpineol may induce morphostructural alterations in Escherichia coli. Brazilian Journal of Microbiology. 2014;45(4):1409–13.
16. Kong Q, Zhang L, An P, Qi J, Yu X, Lu J, Ren X. Antifungal mechanisms of α-terpineol and terpene-4-alcohol as the critical components of Melaleuca alternifolia oil in the inhibition of rot disease caused by Aspergillus ochraceus in postharvest grapes. Journal of applied microbiology. 2019;126(4):1161–74.
17. ud Din F, Aman W, Ullah I, Qureshi OS, Mustapha O, Shafique S, et al. Effective use of nanocarriers as drug delivery systems for the treatment of selected tumors. International Journal of Nanomedicine. 2017;12:7291.
18. Dong W, Ye J, Wang W, Yang Y, Wang H, Sun T, Gao L, Liu Y. Self-assembled lecithin/chitosan nanoparticles based on phospholipid complex: a feasible strategy to improve entrapment efficiency and transdermal delivery of poorly lipophilic drug. International Journal of Nanomedicine. 2020;15:5629–43.
19. van Hoogevest P. Review–an update on the use of oral phospholipid excipients. European Journal of Pharmaceutical Sciences. 2017;108:1–12.
20. Drescher S, van Hoogevest P. The phospholipid research center: current research in phospholipids and their use in drug delivery. Pharmaceutics. 2020;12(12):1235.
21. Khan MM, Madni A, Torchilin V, Filipczak N, Pan J, Tahir N, Shah H. Lipid-chitosan hybrid nanoparticles for controlled delivery of cisplatin. Drug Delivery. 2019;26(1):765–72.
22. Aibani N, Rai R, Patel P, Cuddihy G, Wasan EK. Chitosan nanoparticles at the biological interface: implications for drug delivery. Pharmaceutics. 2021;13(10):1686.
23. Prabaharan M. Chitosan-based nanoparticles for tumor-targeted drug delivery. International Journal of Biological Macromolecules. 2015;72:1313–22.
24. Özcan İ, Azizoğlu E, Şenyiğit T, Özyazıcı M, Özer Ö. Enhanced dermal delivery of diflucortolone valerate using lecithin/chitosan nanoparticles: in-vitro and in-vivo evaluations. International Journal of Nanomedicine. 2013;8:461.
25. Ma Q, Gao Y, Sun W, Cao J, Liang Y, Han S, Wang X, Sun Y. Self-assembled chitosan/phospholipid nanoparticles: from fundamentals to preparation for advanced drug delivery. Drug Delivery. 2020;27(1):200–15.
26. Ramasamy T, Tran TH, Cho HJ, Kim JH, Kim YI, Jeon JY, Choi HG, Yong CS, Kim JO. Chitosan-based polyelectrolyte complexes as potential nanoparticulate carriers: physicochemical and biological characterization. Pharmaceutical Research. 2014;31(5):1302–14.
27. Veronese FM, Pasut G. PEGylation, successful approach to drug delivery. Drug Discovery Today. 2005;10(21):1451–8.
28. Kouchakzadeh H, Shojaosadati SA, Maghsoudi A, Farahani EV. Optimization of PEGylation conditions for BSA nanoparticles using response surface methodology. Aaps Pharmscitech. 2010;11(3):1206–11.
29. Marques SS, Ramos II, Fernandes SR, Barreiros L, Lima SA, Reis S, et al. Insights on ultrafiltration-based separation for the purification and quantification of methotrexate in nanocarriers. Molecules. 2020;25(8):1879.
30. Hosseini SF, Zandi M, Rezaei M, Farahmandghavi F. Two-step method for encapsulation of oregano essential oil in chitosan nanoparticles: preparation, characterization and in vitro release study. Carbohydrate Polymers. 2013;95(1):50–6.
31. Valencia MS, da Silva Júnior MF, Xavier-Júnior FH, de Oliveira VB, de Albuquerque PBS, de Oliveira Borba EF, et al. Characterization of curcumin-loaded lecithin-chitosan bioactive nanoparticles. Carbohydrate Polymer Technologies and Applications. 2021;2:100119.
32. Pumiputavon K, Chaowasku T, Saenjum C, Osathanunkul M, Wungsintaweekul B, Chawansuntati K, Wipasa J, Lithanatudom P. Cell cycle arrest and apoptosis induction by methanolic leaves extracts of four Annonaceae plants. BMC Complementary and Alternative Medicine. 2017;17(1):1–11.
33. Mudunkotuwa IA, Al Minshid A, Grassian VH. ATR-FTIR spectroscopy as a tool to probe surface adsorption on nanoparticles at the liquid–solid interface in environmentally and biologically relevant media. Analyst. 2014;139(5):870–81.
34. Guo Q, Ai L, Cui SW. Fourier transform infrared spectroscopy (FTIR) for carbohydrate analysis. In: Methodology for Structural Analysis of Polysaccharides: Springer; 2018. p. 69–71.
35. Perez-Ruiz AG, Ganem A, Olivares-Corichi IM, García-Sánchez JR. Lecithin–chitosan–TPGS nanoparticles as

nanocarriers of (−)-epicatechin enhanced its anticancer activity in breast cancer cells. RSC Advances. 2018;8(61):34773–82.

36. Vrandečić NS, Erceg M, Jakić M, Klarić I. Kinetic analysis of thermal degradation of poly (ethylene glycol) and poly (ethylene oxide) s of different molecular weight. Thermochimica Acta. 2010;498(1-2):71–80.

37. Mahmood S, Kiong KC, Tham CS, Chien TC, Hilles AR, Venugopal JR. PEGylated lipid polymeric nanoparticle–encapsulated acyclovir for in vitro controlled release and ex vivo gut sac permeation. AAPS PharmSciTech. 2020;21(7):1–15.

38. Bose SK, Nirbhavane P, Batra M, Chhibber S, Harjai K. Nanolipoidal α-terpineol modulates quorum sensing regulated virulence and biofilm formation in Pseudomonas aeruginosa. Nanomedicine. 2020;15(18):1743–60.

39. Altmeyer C, Karam TK, Khalil NM, Mainardes RM. Tamoxifen-loaded poly (L-lactide) nanoparticles: development, characterization and in vitro evaluation of cytotoxicity. Materials Science and Engineering: C. 2016;60:135–42.

40. Alves ACS, Mainardes RM, Khalil NM. Nanoencapsulation of gallic acid and evaluation of its cytotoxicity and antioxidant activity. Materials Science and Engineering: C. 2016;60:126–34.

41. Martins LG, Mainardes RM. Application of a validated HPLC-PDA method for the determination of melatonin content and its release from poly (lactic acid) nanoparticles. Journal of Pharmaceutical Analysis. 2017;7(6):388–93.

42. Jiang L, Sheikh MS, Huang Y. Decision making by p53: life versus death. Molecular and Cellular Pharmacology. 2010;2(2):69–77.

43. Sharma MR, Tuszynski GP, Sharma MC. Angiostatin-induced inhibition of endothelial cell proliferation/apoptosis is associated with the down-regulation of cell cycle regulatory protein cdk5. Journal of Cellular Biochemistry. 2004;91(2):398–409.

44. Kastan MB, Canman CE, Leonard CJ. P53, cell cycle control and apoptosis: implications for cancer. Cancer and Metastasis Reviews. 1995;14(1):3–15.

45. Tyavambiza C, Elbagory AM, Madiehe AM, Meyer M, Meyer S. The antimicrobial and anti-inflammatory effects of silver nanoparticles synthesised from Cotyledon orbiculata aqueous extract. Nanomaterials. 2021;11(5):1343.

46. Ilk S, Saglam N, Özgen M. Kaempferol loaded lecithin/chitosan nanoparticles: preparation, characterization, and their potential applications as a sustainable antifungal agent. Artificial Cells, Nanomedicine, and Biotechnology. 2017;45(5):907–16.

47. Liu L, Zhou C, Xia X, Liu Y. Self-assembled lecithin/chitosan nanoparticles for oral insulin delivery: preparation and functional evaluation. International Journal of Nanomedicine. 2016;11:761.

48. Naskar S, Kuotsu K, Sharma S. Chitosan-based nanoparticles as drug delivery systems: a review on two decades of research. Journal of Drug Targeting. 2019;27(4):379–93.

49. Maiti R, Panigrahi S, Yin T, Huo M. Bovine serum albumin nanoparticles constructing procedures on anticancer activities. Int J Adv Res Biol Sci. 2018;5(4):226–39.

50. Şenyiğit T, Sonvico F, Barbieri S, Özer Ö, Santi P, Colombo P. Lecithin/chitosan nanoparticles of clobetasol-17-propionate capable of accumulation in pig skin. Journal of Controlled Release. 2010;142(3):368–73.

51. Mariyam M, Ghosal K, Thomas S, Kalarikkal N, Latha MS. Dendrimers: general aspects, applications and structural exploitations as prodrug/drug-delivery vehicles in current medicine. Mini Reviews in Medicinal Chemistry. 2018;18(5):439–57.

52. Barbieri S, Sonvico F, Como C, Colombo G, Zani F, Buttini F, Bettini R, Rossi A, Colombo P. Lecithin/chitosan controlled release nanopreparations of tamoxifen citrate: loading, enzyme-trigger release and cell uptake. Journal of Controlled Release. 2013;167(3):276–83.

53. Hafner A, Dürrigl M, Pepić I, Filipović-Grčić J. Short-and long-term stability of lyophilised melatonin-loaded lecithin/chitosan nanoparticles. Chemical and Pharmaceutical Bulletin. 2011;59(9):1117–23.

54. Moreno E, Schwartz J, Larrea E, Conde I, Font M, Sanmartín C, Irache JM, Espuelas S. Assessment of β-lapachone loaded in lecithin-chitosan nanoparticles for the topical treatment of cutaneous leishmaniasis in L. major infected BALB/c mice. Nanomedicine: Nanotechnology, Biology and Medicine. 2015;11(8):2003–12.

55. Pereira MC, Oliveira DA, Hill LE, Zambiazi RC, Borges CD, Vizzotto M, Mertens-Talcott S, Talcott S, Gomes CL. Effect of nanoencapsulation using PLGA on antioxidant and antimicrobial activities of guabiroba fruit phenolic extract. Food Chemistry. 2018;240:396–404.

56. Zengin H, Baysal AH. Antibacterial and antioxidant activity of essential oil terpenes against pathogenic and spoilage-forming bacteria and cell structure-activity relationships evaluated by SEM microscopy. Molecules. 2014;19(11):17773–98.

57. Souza MP, Vaz AF, Correia MT, Cerqueira MA, Vicente AA, Carneiro-da-Cunha MG. Quercetin-loaded lecithin/chitosan nanoparticles for functional food applications. Food and Bioprocess Technology. 2014;7(4):1149–59.

58. Alhajamee M, Marai K, Al Abbas SMN, Homayouni TM. Co-encapsulation of curcumin and tamoxifen in lipid-chitosan hybrid nanoparticles for cancer therapy. Materials Technology. 2021:1–12.

59. Brunetti J, Carnicelli V, Ponzi A, Di Giulio A, Lizzi AR, Cristiano L, et al. Antibacterial and anti-inflammatory activity of an antimicrobial peptide synthesized with D amino acids. Antibiotics. 2020;9(12):840.

60. Pandya S. Nanoemulsion and their antimicrobial activity. Researchgate publications. 2015. https://doi.org/10.13140/RG.2.1.2274.6961.

61. Chen L, Deng H, Cui H, Fang J, Zuo Z, Deng J, Li Y, Wang X, Zhao L. Inflammatory responses and inflammation-associated diseases in organs. Oncotarget. 2018;9(6):7204–18.

62. Khaleel C, Tabanca N, Buchbauer G. α-Terpineol, a natural monoterpene: a review of its biological properties. Open Chemistry. 2018;16(1):349–61.

63. Itani WS, El-Banna SH, Hassan SB, Larsson RL, Bazarbachi A, Gali-Muhtasib HU. Anti colon cancer components from lebanese sage (Salvia libanotica) essential oil: mechanistic basis. Cancer Biology & Therapy. 2008;7(11):1765–73.

64. Hobbs SK, Monsky WL, Yuan F, Roberts WG, Griffith L, Torchilin VP, Jain RK. Regulation of transport pathways in tumor vessels: role of tumor type and microenvironment. Proceedings of the National Academy of Sciences. 1998;95(8):4607–12.

65. Maeda H. The enhanced permeability and retention (EPR) effect in tumor vasculature: the key role of tumor-selective macromolecular drug targeting. Advances in Enzyme Regulation. 2001;41:189–207.

66. Ahmed NH, Said UZ, Meky NH, Mohamed MA. Role of chitosan nanoparticles as anti-angiogenic in mice bearing Ehrlich carcinoma. Oncol Res Rev. 2018;1:1–6.

67. Dragostin O-M, Tatia R, Samal SK, Oancea A, Zamfir AS, Dragostin I, Lisă EL, Apetrei C, Zamfir CL. Designing of chitosan derivatives nanoparticles with antiangiogenic effect for cancer therapy. Nanomaterials. 2020;10(4):698.

68. Zhang L, Hu Y. Alphastatin-loaded chitosan nanoparticle preparation and its antiangiogenic effect on lung carcinoma. International Journal of Polymer Science. 2019;2019:1–9.